

Low-loss Hollow-core Waveguide using High-Contrast Sub-wavelength Grating

James Ferrara^a, Weijian Yang^a, Anthony Yeh^a, Karen Grutter^a,
Christopher Chase^a, Vadim Karagodsky^a, Devang Parekh^a, Yang Yue^b,
Alan E. Willner^b, Ming C. Wu^a and Connie J. Chang-Hasnain^{*a}

^aDept. of EECS, University of California at Berkeley, Berkeley, CA 94720, USA;

^bDept. of Elect. Engineering, University of Southern California, Los Angeles, CA 90089, USA

ABSTRACT

We present a novel form of hollow-core waveguiding that enables chip-scale integration. Light propagates in air along a zig-zag path between very highly-reflective Si metastructures comprised of a single layer of sub-wavelength high-contrast gratings (HCGs) without the aid of sidewalls. Top and bottom subwavelength HCGs separated by 9 μ m of air and with periodicity perpendicular to the propagation of light reflect light at shallow angles with extremely low loss. The HCGs are patterned on SOI wafers with 340 nm-thick Si device layers engraved in a single etch step, and have been measured to have a 0.37 dB/cm propagation loss. Our work demonstrates the light-guiding properties of HCG hollow-core waveguides with a novel form of lateral beam confinement that uses subtle reflection phase changes between core and cladding HCG regions capable of bending light around 30 mm radius-of-curvature tracks.

Keywords: Hollow-core waveguide, HCW, high-contrast grating, HCG, infrared gas-sensing, silicon photonics

1. INTRODUCTION

Over the past few years, hollow-core waveguides (HCWs) have received much attention for their properties at wavelengths where traditional solid waveguides encounter difficulties, such as excessive optical absorption and undesirable non-linear effects. As gas sensors¹, they can provide an alternative to integrated-circuit technology, where electromagnetic interference and high temperature environments can be detrimental. Other applications include infrared high-power optical delivery and non-linear optics, where high beam intensities and long interaction lengths are desirable for increased light-matter interactions^{2,3}. Many designs have been shown to efficiently confine light in a hollow-core waveguide such as photonic crystal fibers^{4,5}, DBR reflectors⁶, and ARROW waveguides^{7,8}. However, the reflection principles for these hollow-core waveguides require interactions with multiple layers of very precisely laid-out films, which can be cumbersome to fabricate and make them nearly impossible to form integrated optical components.

In this work, we present a novel form of hollow-core waveguiding that enables the possibility of chip-scale integration of light sources, detectors and electronics on a silicon platform. In an HCW, an optical beam is guided along a low-index medium by zig-zag reflections of the guiding walls^{6,9}. To attain low propagation losses, the sidewall reflectivity must be exceptionally high at the propagating wavelengths due to large numbers of bounces per unit length. High contrast subwavelength gratings (HCGs) have been found to offer very high reflection for surface-normal incident light¹⁰⁻¹³, and recently, we reported numerical simulation results of a one-dimensional (1D) waveguide guided by two parallel layers of HCGs whose periodicity is parallel to the direction of propagation⁹. Top and bottom subwavelength HCGs separated by air and with periodicity perpendicular to the propagation of light are capable of reflecting light at shallow angles with extremely low loss. Our work demonstrates the light-guiding properties of HCG hollow-core waveguides with a novel form of lateral beam confinement that employs the effective index guiding method¹⁴. HCG HCWs are capable of bending light around curves without the aid of sidewalls. The lack of sidewalls is especially attractive for applications where gases or fluids have difficulty flowing into a device due to small core openings. The increase in speed for these waveguides can be increased by a factor of L^2/d^2 , where the length L can be several orders of magnitude greater than d .

*cch@eecs.berkeley.edu

2. HCG HCW DESIGN AND FABRICATION

Two parallel planar wafers are used to define straight and curved HCG HCWs, each containing a single layer of HCGs. The guided wave propagates along the HCG grating bars, as shown schematically in Fig. 1a, with lateral guidance provided by subtle HCG dimension variations that create an effective refractive index variation to confine light within a single mode. The design method is simple and intuitive, and does not require lengthy numerical simulation. The propagation loss in a straight waveguide with a 9- μm waveguide height is measured to be 0.37 dB/cm, the lowest loss for a small core HCW.

An HCG structure consists of a single layer of grating made from a high-refractive-index material (such as silicon), fully surrounded by a low-refractive-index material (such as air or oxide). They have been shown to be high reflection mirrors at normal incident angle for vertical-cavity surface-emitting lasers (VCSELs)¹¹⁻¹³. Simulations show that HCGs retain their high reflection and wide bandwidth properties for glancing angles as well⁹. In this work, we demonstrate a rather counter-intuitive configuration with the propagation direction of the guided light being *parallel* to the HCG grating bars.

Fabricated on a silicon-on-insulator (SOI) platform, the gratings are formed on the silicon device layer above silicon dioxide (SiO_2). By placing two HCG-patterned wafers in parallel, separated by an air-gap d (shown schematically in Fig. 1a), we have an HCW with the added freedom of controlling the waveguide core height d . The device arrangement provides a dynamic understanding of the HCG waveguiding concept, allowing for d to be varied in-measurement. Monolithic integration of HCG HCWs can be made possible through various bonding schemes or by using sophisticated multi-layer SOI wafer topologies.

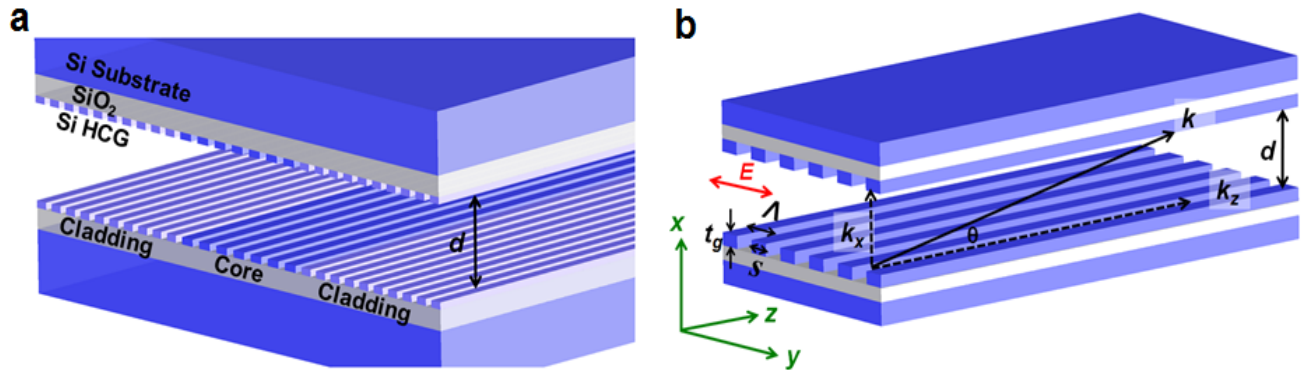


Figure 1. The HCG HCW. **a**, Schematic of an HCG HCW. The silicon HCG sits on top of a SiO_2 layer and silicon substrate. Two HCG chips are placed in parallel with a separation gap d , forming an HCW. In the lateral direction, the core and cladding are defined by different HCG parameters to provide lateral confinement. **b**, Ray optics illustration for a 1D slab HCG HCW. The \mathbf{k} vector is decomposed into the propagation constant k_z and transverse component k_x . θ is the angle between \mathbf{k} and k_z ; d is the waveguide height; \mathbf{E} indicates the oscillation direction of the electrical field; λ is the HCG period; s is the silicon grating bar width and t_g is the HCG thickness.

The waveguide design begins with a 1D model using simple ray optics⁹. The propagation loss and the effective refractive index n_{eff} of the fundamental waveguide mode are given by:

$$Loss \left[\frac{\text{dB}}{\text{m}} \right] = -10 \frac{\tan \theta}{d_{eff}} \log_{10} |r|^2 \quad (1)$$

$$n_{eff} = \cos \theta = \frac{k_z}{k} \quad (2)$$

As illustrated in Fig. 1b, θ is the angle between the ray and the waveguide, k_z is the propagation constant, k is the wave vector of the light in free space, and d_{eff} is the effective waveguide height. d_{eff} takes into account both the physical waveguide height d and the reflection phase φ_r , which is approximately π in general. The parameter d_{eff} can be calculated by the round-trip phase condition of the fundamental mode:

$$2k_x d + 2\varphi_r = 4\pi \quad (3)$$

$$2k_x d + 2\varphi_r = 2k_x d_{eff} + 2\pi \quad (4)$$

For solid-core waveguides, a typical lateral guiding design employed is the effective index method¹⁵, that uses different k_z values in the core and cladding region. Here, we also propose the same -- obtaining lateral confinement by using different HCG designs for the core and cladding region so that the effective refractive index of the core is higher than that of the cladding⁹. This can be achieved by fine-tuning the HCG reflection phase, φ_r , which determines the effective index n_{eff} of the 1D-slab waveguide in Eq. (2)-(4). The 2D waveguide is a piece-wise composition of 1D HCG slab waveguides (forming an HCG double heterostructure, i.e. cladding/core/cladding), with the condition that both HCGs designs have high reflectivity. To maintain a flat structure, we consider only a single HCG thickness t_g , for both core and cladding designs. Even with this limitation, HCG designs with different periods Λ and grating widths s can provide remarkably large differences in φ_r , while maintaining a high reflectivity; this results in a *variation in effective refractive index between HCG designs on a flat surface*.

2.1 RCWA Simulations

Rigorous coupled wave analysis¹⁵ is used to calculate the complex reflection coefficient r of the HCG. r is calculated for different HCG periods Λ and silicon grating bar widths for discrete HCG thicknesses. At a t_g of 340 nm, on a 2- μ m-thick layer of buried oxide the incidence angle of the light on the HCG is 85.06°, corresponding to the angle between the light ray and the normal of the HCG reflector in a 9- μ m waveguide, and an HCG reflection phase φ_r of π . The wavelength of the light is 1550 nm, and the light polarization is TE from the perspective of the waveguide. Based on the ray optics for an HCW, r is converted into the propagation loss, as well as the effective refractive index n_{eff} of the 1D slab waveguide's fundamental mode using Eq. (1)-(4). Equivalently, finite element method (FEM) can be used to simulate the propagation mode of the HCG hollow-core slab waveguide, and propagation loss and effective refractive index can be extracted. Fig. 2 shows the contour plot of loss and effective refractive index calculated by FEM. This provides the design template for glancing angle HCG.

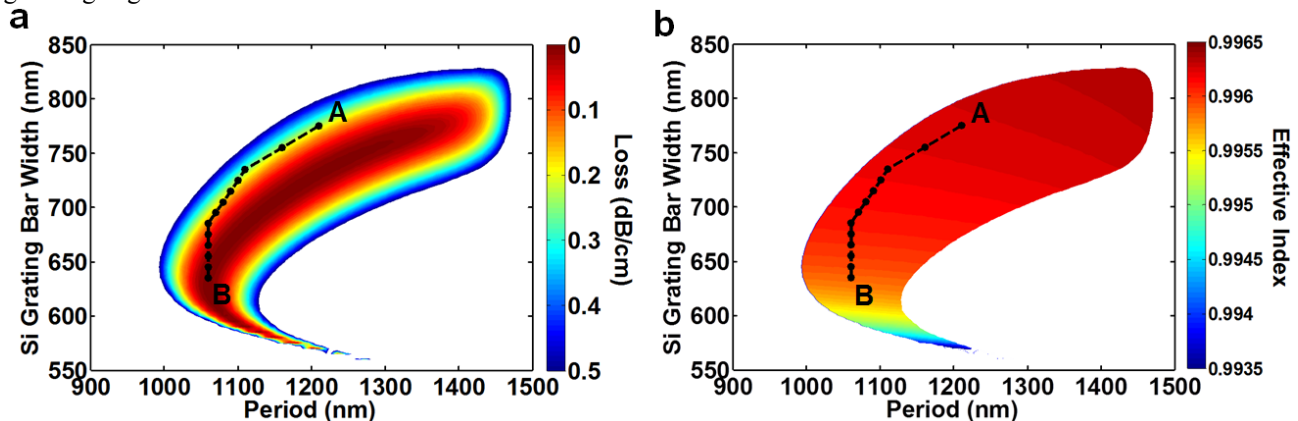


Figure 2. Loss and effective index contour plots of HCG hollow-core slab waveguides at d of 9- μ m. The contour plots provide the design template for the waveguide. Different HCG periods Λ and silicon grating bar widths s are chosen for the core (point A) and cladding (point B), as well as the transition region (dots linked with dashed lines). The HCG thickness t_g is fixed at 340 nm, and the buried oxide thickness is set to 2 μ m. The wavelength of the light is 1550 nm.

We design the HCG period and silicon bar width to be 1210 nm and 775 nm for the core region, and 1060 nm and 635 nm for the cladding region. Also known for solid core waveguides, graded-index waveguides typically exhibit lower loss than step-index waveguides¹⁶. A graded effective-index profile is introduced by chirping HCG dimensions on the order of tens nanometers (gradually changing parameters from A to B, in Fig.2). The core width W_c and the transition

region width W_i are 10.9 μm and 11.9 μm respectively. The cladding width of the waveguide is 42.7 μm on each side. The relative effective refractive index difference between the core and cladding is 0.04%.

Fig 3a shows the simulated mode profile of the fundamental mode of a 2D HCG HCW, simulated by FEM. The mode effective refractive index is simulated to be 0.9961 and propagation loss 0.35 dB/cm at 1550 nm. The minimum loss is 0.31 dB/cm at 1535 nm. It is truly remarkable to note that, although the guided mode has very little energy in the HCGs, the effective index model can be used and obtained with simple and small parameter changes of the HCG.

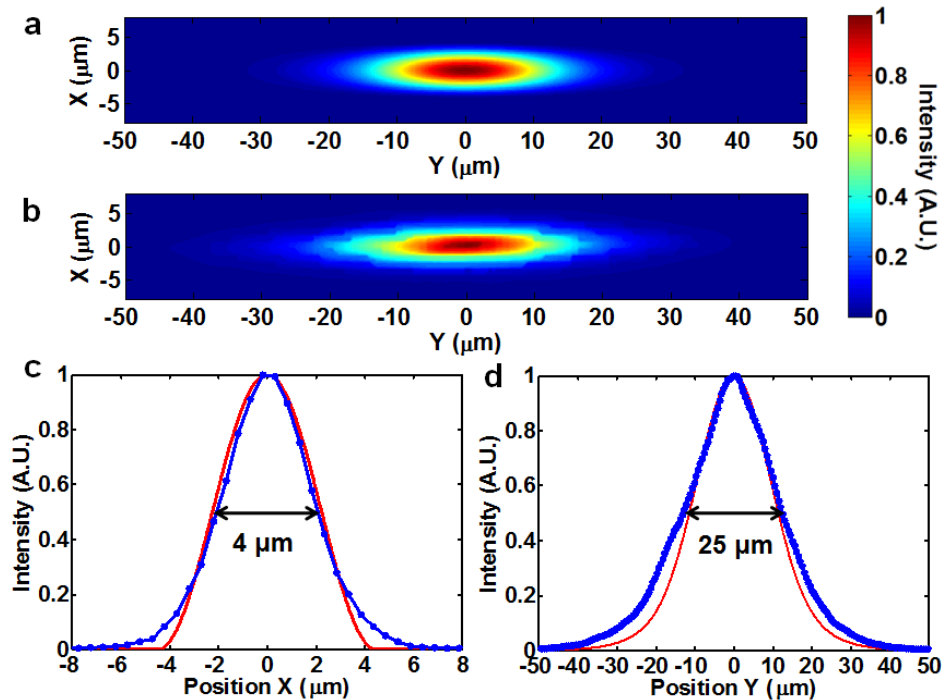


Figure 3. Optical mode of an HCG HCW. **a**, Propagation mode profile simulated by FEM. **b**, The measured mode profile from the fabricated device. **c**, Transverse and **d**, lateral mode profile. The simulation (red curve) agrees well with experiment (blue line). The full width at half maximum (FWHM) is 4 μm in the transverse direction, and 25 μm in the lateral direction. The wavelength in both simulation and measurement is 1550 nm

2.2 HCG HCW Fabrication

The HCG HCW was fabricated using deep ultra-violet lithography on 6-inch SOI wafers, followed by a standard silicon inductively coupled plasma reactive-ion etching (ICP-RIE) process. The great advantage of this lateral confinement scheme is that only a single etching step is required. Fig. 4 shows the top-view optical microscope image of the fabricated chips (a) as well as the scanning electron microscope image of the HCG in the core (b) and cladding (c) region. The core, transition, and cladding regions of the waveguide can be clearly distinguished under the optical microscope. The HCG grating bars have a smooth surface and a sidewall roughness of about 10 nm. The period and silicon grating bar width of the HCG are in agreement with the design values, and the silicon grating bar width varies by $\leq \pm 1.5\%$ across the 6-inch wafer. For loss measurements, the waveguides are cut into different lengths and two pieces of patterned HCG chips are then mounted onto two translation stages. The stages are aligned and brought close together to form the HCG HCW.

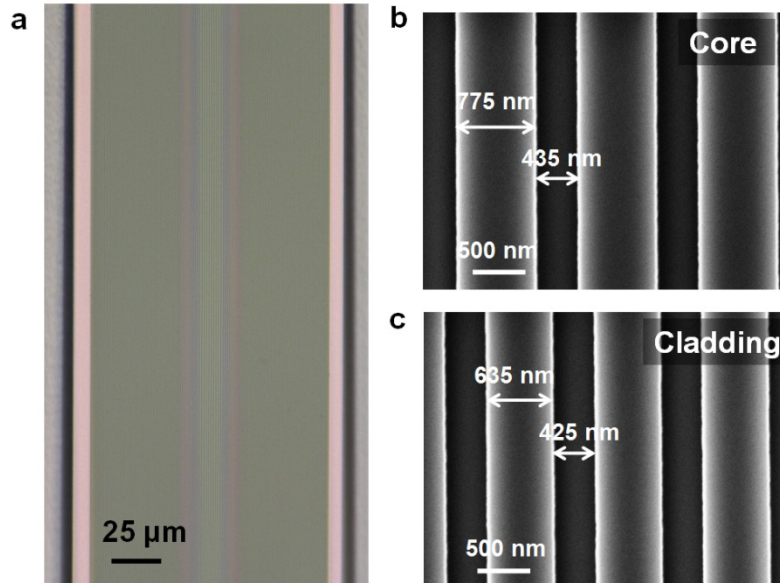


Figure 4. Fabricated HCG HCW chips. **a**, Optical microscope image of the HCG chip. The core, transition and cladding regions are clearly distinguished by their diffracted colors. **b**, **c** The SEM image of the HCG grating bars in the core region and cladding regions.

3. EXPERIMENTAL RESULTS

3.1 Optical mode imaging and loss measurement

To characterize the light guiding in the HCG HCW, a laser beam from a tunable laser source is first polarization adjusted and then collimated by a fiber collimator, and launched into the HCG HCW sample by a 10X objective. A 50X objective is used to collect the light for output facet imaging. With precise alignment of the two chips, an optical mode can be seen at the output facet. Fig. 3b shows the output image with the waveguide height d set to 9 μm . The measured profiles in the transverse and lateral direction are shown in Figs. 3c and 3d with 4 μm and 25 μm full width at half maximum (FWHM), respectively, at a wavelength of 1550 nm. Excellent agreement is obtained between simulation and experiment.

For loss measurement, the laser is internally modulated at 1 kHz. The 50X objective is replaced with a photodetector that butt-couples the light from the waveguide in order to allow the optical power to be measured with a lock-in amplifier.

3.2 Data Processing for Waveguide Loss

A cut-back method is applied to extract the net propagation loss and the coupling loss of the HCG HCW. The loss spectrum of the whole optical path is first measured without the HCG HCW. The total loss spectrum is then measured for different lengths of waveguides. As mentioned above, due to the fabrication variation across the 6-inch SOI wafer, the HCG dimensions are not identical on all different pieces of waveguides. The silicon grating bar width varies by $<\pm 1.5\%$ across the 6-inch wafer. This leads to a shift of the loss spectra (<20 nm with respect to the wavelength) between different pieces of waveguides. To improve the accuracy of the cut-back method, the loss spectra for the four different waveguide lengths are aligned in a range according to their minimum loss values. The net propagation loss is extracted for each wavelength based on a linear fit for the total loss of the four different lengths, and the propagation loss spectrum is obtained.

Fig. 5a shows the measured total loss spectrum for straight waveguides with lengths of 18 mm, 38 mm, 58 mm and 78 mm. The extracted propagation loss spectrum agrees well with the results of the simulation. The minimum loss value from experiment is 0.37 dB/cm at 1535 nm, slightly higher than the simulated value. This difference is attributed to a slight warping of the two HCG chips across their length, which leads to some variation of core height on the order of ± 1 μm . In addition, the HCG surface scattering loss may contribute to additional loss. The coupling loss is estimated to

be 4 dB, which can be further reduced by improving the coupling region. By optimizing the HCG dimensions and waveguide layout, an even lower loss can be expected.

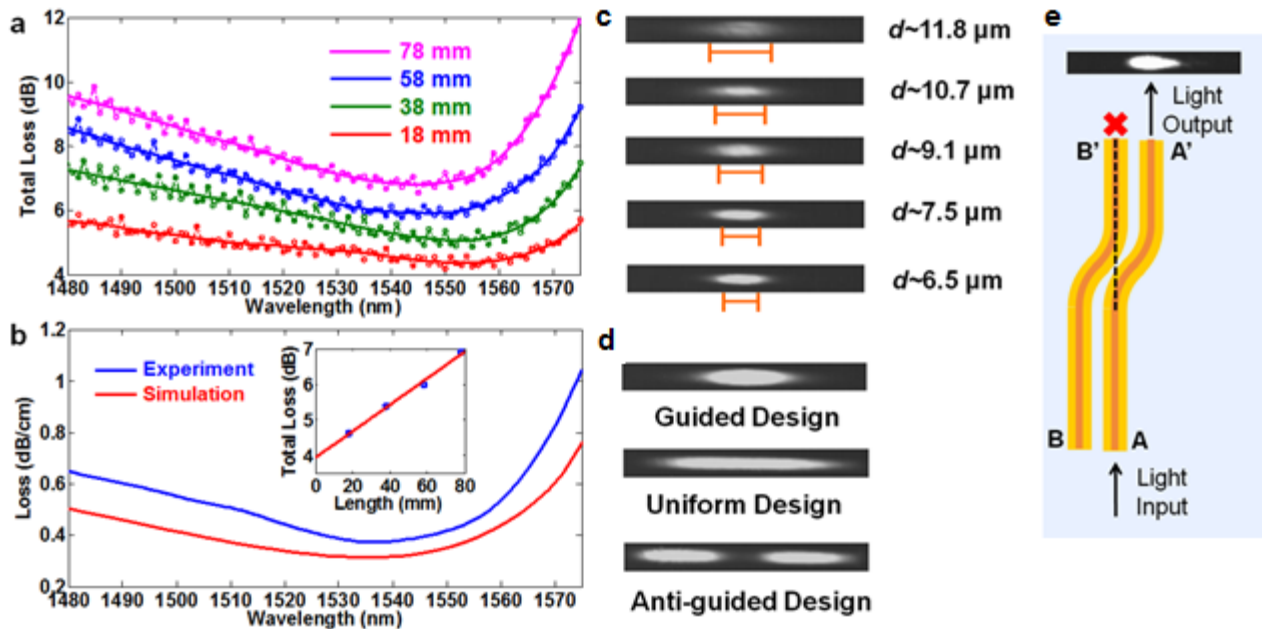


Figure 5. Loss spectrum of the HCG HCW for a 9- μm -high waveguide and lateral confinement. **a**, Total loss spectrum for an HCG HCW with four different lengths. The dashed dot line is the measured data. The oscillation is due to the laser and a residual Fabry-Perot cavity in the optical path of the measurement system. To remove this noise, a smoothing spline method is applied and the solid curves show the clean spectra. **b**, The experimental extracted propagation loss as a function of wavelength (blue) and the simulated loss spectrum obtained by FEM (red). Inset: the linear curve fitting used to extract the propagation loss and coupling loss at 1535 nm. **c**, Mode profile at different waveguide heights d . As d decreases, $\Delta n/n_{\text{core}}$ increases, and the mode is more confined with reduced lateral leakage. The guidelines indicate the FWHM of the mode in the lateral direction. **d**, Mode profiles for three side-by-side HCWs, with lateral guiding (top), step-index guiding (middle) and anti-guided design where the core and cladding designs are swapped (bottom). For the mode profiles, the output power of the mode is kept constant and d is constant $\sim 9 \mu\text{m}$. The image window is $140 \mu\text{m}$ by $16 \mu\text{m}$. The wavelength is set to 1550 nm. **e**, Layout of the curved waveguides. Curved waveguides A-A' and B-B' are parallel, and the input port of A-A' is aligned with the output port of B-B'. Light is launched into port A. Light guiding by the bend is demonstrated with the output observed in A' rather than B'.

3.3 Dependence of Lateral Confinement on Core Height d

The effective index method is the main concept for the proposed lateral confinement scheme. It is further tested and illustrated by varying the waveguide height d . As seen in Fig. 1b and Eq. (3-4), for a round trip in the transverse direction, the beam acquires phase through two components: interaction with the HCG (associated with a phase of $2\phi_r$) and travel through the air trajectory (associated with a phase of $2k_x d$). Since the latter component is nearly constant for both the core and cladding regions, the HCG phase component creates the effective index difference ($\Delta n/n_{\text{core}}$). As d reduces, the contribution from the HCG increases relative to the air contribution, and thus $\Delta n/n_{\text{core}}$ becomes more pronounced. This results in a stronger lateral confinement and a narrowing of mode with reduced d , as illustrated in Fig. 5c with experimental measured mode profiles versus d .

To further illustrate lateral index guiding, we fabricated various waveguides on the same chip with step-index guiding (uniform HCG design) and anti-guiding (with swapped core and cladding designs from the original). The output mode profiles are presented in Fig. 5d, and they show distinct differences with light dispersed in the waveguide without the appropriate HCG design. These lateral confinement measurements demonstrate the effectiveness of the effective index method for an HCW for the first time. It is truly remarkable that with little optical energy in the HCG, lateral guiding can be obtained with a planar structure. This enables light to be guided in an HCW without the aid of physical side reflectors, and opens up a new regime of optical waveguiding.

3.4 Light Guiding in Curved HCG HCWs

Light can also bend and stay guided by this sidewall-less waveguides. Fig. 5e shows a top view of the curved waveguide layout. For very large d , light launched into port A of the waveguide is observed at both A' and B' output ports, a result of weak lateral confinement. As d is decreased, the lateral confinement mechanism is strengthened, as described in 3.3, and light output at port B is quenched. The mode profile in Fig. 5e shows light output only observed at port A'. We fabricated and confirmed well-confined modes for curved waveguides with 80 mm, 50 mm, and 30 mm radii-of-curvature (ROC).

4. CONCLUSION

The ability to engineer the phase response of a planar HCG double heterostructure has led to the development of low-loss HCG HCWs on silicon. These waveguides feature a lateral confinement scheme that is unique to them in that they do not require sidewalls to maintain a well-defined lateral mode, a property that makes them particularly attractive for use in compact, low-power, fast on-chip gas/fluid sensing applications. Typical HCWs used in gas/fluid sensing experiments are limited by the long diffusion times of molecules into the waveguided region, where only the input and output ends serve as inlets. Other setups require separate bulky pumping devices that increase the complexity of the system. With no sidewalls, gaseous or fluidic molecules can penetrate into the HCG HCW nearly instantaneously when compared to conventional HCW counterparts. Other potential applications for waveguides that allow dispersion engineering include radio-frequency (RF) filters and low noise oscillators, optical routers and couplers based on multi-mode interference, among others.

We present the first experimental device showing lateral confinement in a low-loss planar HCW structure. The planar structure of the HCG makes fabrication simple, only a single etching step is required. Although the waveguides presented here offer a proof-of-concept, monolithic integration of the HCG double heterostructures is possible by flip-chip bonding, or by processing on a multi-stack SOI wafer. The HCG designs are chosen through straightforward slab waveguide numerical simulations in conjunction with the effective index method, both of which are experimentally confirmed in an HCW. The measured propagation loss is the lowest among all HCWs that are mode-matched to a single-mode optical fiber, and with further optimization of the HCG dimensions based on the loss contour and effective index contour map losses can be lower than 0.1 dB/cm in FEM simulations. In closing, this unique HCG HCW lateral confinement mechanism without sidewalls opens up a new scheme of waveguide engineering.

REFERENCES

- [1] Bernini, R. Campopiano, S., Zeni, L., "Silicon micromachined hollow optical waveguides for sensing applications," *IEEE J. Sel. Topics Quantum Electron.*, 8, 106-878 (2002)
- [2] Harrington, J. A., [Selected Papers on Infrared Fiber Optics], SPIE Vol. 9 of Milestone Series, Bellingham, Wash., (1990)
- [3] Saito, Y., Kanaya, T., Nomura, A., Kano, T., "Experimental trial of a hollow-core waveguide used as an absorption cell for concentration measurement of NH₃ gas with a CO₂ laser," *Opt. Lett.*, 18, 2150-2152 (1993).
- [4] Benabid, F., Knight, J. C., Antonopoulos, G., Russell, P. St. J., "Stimulated Raman scattering in hydrogen-filled hollow-core photonic crystal fiber," *Science*, 298, 399-402 (2002).
- [5] Temelkuran, B., Hart, S. D., Benoit, G., Joannopoulos, J. D., Fink, Y., "Wavelength-scalable hollow optical fibres with large photonic bandgaps for CO₂ laser transmission," *Nature*, 420, 650-653 (2002).
- [6] Miura, T., Koyama, F., Matsutani, A., "Modeling and fabrication of hollow optical waveguide for photonic integrated circuits," *Jpn. J. Appl. Phys.*, 41, 4785-4789 (2002).
- [7] Yin, D., Schmidt, H., Barber, J.P., Hawkins, A.R., "Integrated ARROW waveguides with hollow cores," *Opt. Express*, 12, 2710-2715 (2004).
- [8] Yang, W., Conkey, D. B., Wu, B., Yin, D., Hawkins, A., Schmidt, H., "Atomic spectroscopy on a chip," *Nature Photon.*, 1, 331-335 (2007).
- [9] Zhou, Y., Karagodsky, V., Pesala, B., Sedgwick, F. G., Chang-Hasnain, C. J., "A novel ultra-low loss hollow-core waveguide using subwavelength high-contrast gratings," *Opt. Express*, 17, 1508-1517 (2009).

- [10] Mateus, C. F. R., Huang, M. C. Y., Chen, L., Chang-Hasnain, C. J., Suzuki, Y., "Broad-band mirror (1.12–1.62 μm) using a subwavelength grating," *IEEE Photon. Technol. Lett.*, 16, 1676–1678 (2004).
- [11] Huang, M. C. Y., Zhou, Y., Chang-Hasnain, C. J., "A surface-emitting laser incorporating a high-index-contrast subwavelength grating," *Nature Photon.*, 1, 119–122 (2007).
- [12] Chang-Hasnain, C. J., Zhou, Y., Huang, M. C. Y., Chase, C., "High-contrast grating VCSELs," *IEEE J. Sel. Topics Quantum Electron.*, 15, 869-878 (2009).
- [13] Chase, C., Rao, Y., Hofmann, W., Chang-Hasnain, C. J., "1550nm high contrast grating VCSEL," *Opt. Express*, 18, 15461-15466 (2010).
- [14] Knox, R. M., Toullos, P. P., "Integrated circuit for the millimeter through optical frequency range," *Proc. Symp. Submillimeter Wave*, J. Fox and M. H. Schlam, eds. Polytechnic Institute of Brooklyn, 497-516 (1970).
- [15] Moharam, M. G., Gaylord, T. K., "Rigorous coupled-wave analysis of planar-grating diffraction," *J. Opt. Soc. Am.*, 71, 811–818 (1981).
- [16] Hu, J., Feng, N., Carlie, N., Petit, L., Wang, J., Agarwal, A., Richardson, K., Kimerling, L., "Low-loss high-index-contrast planar waveguides with graded-index cladding layers," *Opt. Express*, 15, 14566-14572 (2007).

ACKNOWLEDGEMENTS

The authors acknowledge Professors Eli Yablonovitch, Fumio Koyama and Xiaoxu Deng, Dr. Forrest Sedgwick, and Thomas Camenzind for fruitful discussions. This work was supported by DARPA iPHOD HR0011-09-C-0124. CCH thanks support of DoD National Security Science and Engineering Faculty Fellowship, Chang Jiang Scholar Endowed Chair Professorship and Humboldt Research Award.